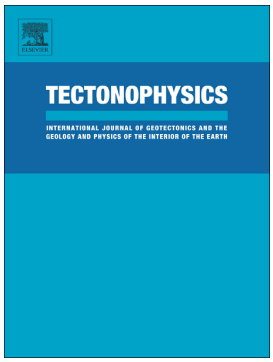

The thermal evolution of Chinese central Tianshan and its implications: Insights from multi-method chronometry

Jiyuan Yin, Wen Chen, Kip V. Hodges, Wenjiao Xiao, Keda Cai, Chao Yuan, Min Sun, Li-Ping Liu, Matthijs C. van Soest

PII: S0040-1951(17)30499-7
DOI: doi:10.1016/j.tecto.2017.11.037
Reference: TECTO 127703

To appear in: *Tectonophysics*

Received date: 9 August 2017
Revised date: 19 November 2017
Accepted date: 27 November 2017

Please cite this article as: Jiyuan Yin, Wen Chen, Kip V. Hodges, Wenjiao Xiao, Keda Cai, Chao Yuan, Min Sun, Li-Ping Liu, Matthijs C. van Soest , The thermal evolution of Chinese central Tianshan and its implications: Insights from multi-method chronometry. The address for the corresponding author was captured as affiliation for all authors. Please check if appropriate. Tecto(2017), doi:10.1016/j.tecto.2017.11.037

The thermal evolution of Chinese central Tianshan and its implications: Insights from multi-method chronometry

Jiyuan Yin [a*], Wen Chen [a], Kip V. Hodges [b], Wenjiao Xiao [c, d],
Keda Cai [d], Chao Yuan [e], Min Sun [f], Li-Ping Liu [g], Matthijs C. van Soest [b]

[a] *Laboratory of Isotope Thermochronology, Institute of Geology, Chinese Academy of Geological Sciences, Beijing 100037, China*

[b] *School of Earth and Space Exploration, Arizona State University, P.O. Box 871404, Tempe, AZ 85287–1404, USA*

[c] *State Key Laboratory of Lithospheric Evolution, Institute of Geology and Geophysics, Chinese Academy of Sciences, Beijing, 100029，China;*

[d] *Xinjiang Research Center for Mineral Resources, Xinjiang Institute of Ecology and Geography, Chinese Academy of Sciences, Urumqi, 830011, China;*

[e] *State Key Laboratory of Isotope Geochemistry, Guangzhou Institute of Geochemistry, Chinese Academy of Sciences, Guangzhou, 510640, China*

[f] *The Department of Hong Kong, The University of Hong Kong, Pokflam Road, Hong Kong, China*

[g] *School of Resources and Environmental Engineering, Shandong University of Technology, Zibo 255000, China*

Abstract

The Chinese Tianshan is located in the south of the Central Asian Orogenic Belt and formed during final consumption of the Paleo-Asian Ocean in the late Palaeozoic. In order to further elucidate the tectonic evolution of the Chinese Tianshan, we have established the temperature-time history of granitic rocks from the Chinese Tianshan through a multi-chronological approach that includes U/Pb (zircon), $^{40}Ar/^{39}Ar$ (biotite and K-feldspar), and (U-Th)/He (zircon and apatite) dating. Our data show that the central Tianshan experienced accelerated cooling during the late Carboniferous- to early Permian. Multiple sequences of complex multiple accretionary, subduction and collisional events could have induced the cooling in the Tianshan Orogenic Belt. The new $^{40}Ar/^{39}Ar$ and (U-Th)/He data, in combination with thermal history modeling results, reveal that several tectonic reactivation and exhumation episodes affected the Chinese central Tianshan during middle Triassic (245-210 Ma), early Cretaceous (140-100 Ma), late Oligocene-early Miocene (35-20 Ma) and late Miocene (12-9 Ma). The middle Triassic cooling dates was only found in the central Tianshan. Strong uplift and deformation in the Chinese

* Corresponding author. E-mail address: yinjiyuan1983@163.com (J. Yin).

Tianshan has been limited and localized. It have been concentrated in around major fault zone and the foreland thrust belt since the early Cretaceous. The middle Triassic and early Cretaceous exhumation is interpreted as distal effects of the Cimmerian collisions (i.e. the Qiangtang and Kunlun-Qaidam collision and Lhasa-Qiangtang collision) at the southern Eurasian margin. The Cenozoic reactivation and exhumation is interpreted as a far field response to the India-Eurasia collision and represents the beginning of modern mountain building and denudation in the Chinese Tianshan.

Keywords: Central Asian Orogenic Belt; Thermochronology; Exhumation; Chinese Tianshan; (U-Th)/He

1. Introduction

The Chinese Tianshan is a major part of the southern Central Asian Orogenic Belt (CAOB). It extends from west to east for over 2500 km through Uzbekistan, Tajikistan, Kyrgyzstan, and Kazakhstan to Xinjiang in northwestern China and contains a record of multiple tectonothermal events (Figs. 1a, b; Gao et al., 1998; Windley et al., 2007; Xiao et al., 2008; Xiao and Santosh, 2014). Major tectonostratigraphic domains found within the Chinese Tianshan Orogen were amalgamated during several Paleozoic accretion-collision events related to the progressive closure of the Paleo-Asian Ocean (Buslov et al., 2001; Windley et al., 2007; Xiao et al., 2013). Final assembly of the CAOB took place in the Permian and was accompanied by significant (post-) collisional tectonic and magmatic activity (Wilhem et al., 2012). The modern Tianshan Orogen was formed as an active intracontinental mountain belt characterized by both fold-and-trust faults and strike-slip tectonics (Buslov et al., 2003). Hence, the geology of the Tianshan Orogen provides a rich record of both polyphase Mesozoic deformation and reactivation of major, older structures in the Late Cenozoic (e.g. Allen and Vincent, 1997; De Grave et al., 2007; 2012; Glorie et al., 2011; Glorie and De Grave, 2016). Thermochronology offers a way to constrain the associated cooling and exhumation episodes associated with progressive convergence and closure of the Paleo-Tethys Ocean and subsequent Mesozoic collisions of the Cimmerian blocks (Qiangtang, Lhasa, Karakoram-Pamir) and Cenozoic India-Eurasia collision (Hendrix et al., 1994; Dumitru et al., 2001; Kapp et al., 2003; Roger et al., 2010; Glorie et al., 2011; Metcalfe, 2013; Glorie and De Grave, 2016). However, some of these episodes may also represent far-field effects of the Mongol-Okhotsk Orogenic Belt (MOOB), which was formed by diachronous oceanic closure between Mongolia-North China and Siberia during the Jurassic through Cretaceous (Metelkin et al., 2010, 2012; Wilhem et al., 2012 and references therein). The far-field effects of the MOOB have been considered as one of possible driving forces for the documented Jurassic-Cretaceous cooling and denudation in the Tianshan, although this interpretation have proved controversial (e.g. Jolivet et al., 2010, 2013, and references therein).

Various methods have been used to explore the cause and timing of deformation, uplift, and exhumation in the Tianshan (Windley et al., 1990; Hendrix et al., 1992, 1994; Allen et al., 1993; Yin et al., 1998; Sun et al., 2004). Previous thermochronologic studies have focused on application of the apatite fission-track chronometer (Hendrix et al., 1994; Sobel and Dumitru, 1997; Dumitru et al., 2001; Wang et a., 2009; Zhang et al., 2009; Jolivet et al., 2010; Wang et al., 2017) or the zircon and apatite (U-Th)/He chronometers. Most available zircon and apatite helium dates are from the Kyrgyz Tianshan (Glorie et al., 2010, 2011; De Grave et al., 2011; 2012; 2013; Glorie and De Grave, 2016) and the southwest Tianshan in China (Qiu et al., 2011; Chang et al., 2012; Yu et al., 2014). Available data from the Chinese central Tianshan are comparatively sparse (Jolivet et al., 2010; Lü et al., 2013).

In order to enhance the published thermochronologic dataset and further constrain the thermal evolution and exhumation history of the Chinese Tianshan, we collected 12 granitic samples from the Dushanzi-Kuqa Highway section and Baluntai area in the Chinese central Tianshan (Figs. 2 and 3). We determined U/Pb (zircon), $^{40}Ar/^{39}Ar$ (biotite and K-feldspar), and (U-Th)/He (zircon and apatite) dates for these samples, collectively, these constrain cooling from solidus temperatures to ~ 70˚C (Hodges, 2014 and references therein).

2. Geological setting

The Chinese Tianshan is usually subdivided into four main tectonic units –the North Tianshan Belt (NTB), the Yili Block (YB), the Central Tianshan Block (CTB) and the South Tianshan Belt (STB) –which are separated by three fault systems: the North Tianshan fault, the North Nalati fault, and the South Nalati fault (Fig.1b; Gao et al., 2009; Xiao et al., 2009; 2013). Paleozoic consumption of the North Tianshan and South Tianshan Oceans left a continuous accretionary complex and Paleozoic island arc that constitutes part of the Tianshan orogenic collage (Jahn et al., 2000; Windley et al., 2007; Xiao et al., 2008, 2013). The closures of the North Tianshan Ocean and South Tianshan Ocean resulted in the gradual consumption of surrounding oceanic lithosphere and final amalgamation of the Tianshan by the late Permian (e.g. Windley et al., 2007; Xiao et al., 2013). During the Mesozoic, the Tianshan Orogen was mainly affected by post-collisional deformation formed of large-scale strike-slip faults resulting from far-field tectonic effects of different collisions. This far field effect could originate at the southern Eurasian margin and/or possibly at the Mongol-Okhotsk Orogeny (Windley et al., 2007; Jolivet et al., 2010; Choulet et al., 2011; Wilhem et al., 2012; De Grave et al., 2013; De Pelsmaeker et al., 2015). The major faults in the Tianshan Orogen were reactivated during the Cenozoic, likely due to the continuing closure of the Tethys Ocean and associated accretions of island-arcs and/or India-Eurasia collision (Glorie et al., 2011; Glorie and De Grave, 2016).

3. Sampling and methods

One of the most effective ways to explore the thermal history of an orogenic environment is the application of multiple isotopic thermochronometers to a single sample. Many lithologies from the central Tianshan are useful to such studies, particularly biotite granite, monzonitic granite and diorite, which contain a wide variety of major and accessory minerals. In this study, we collected twelve granite samples along Dushanzi-Kuqa highway from north to south and around Baluntai town within the central Tianshan (Figs. 2 and 3). Sample details – including location, lithology and isotopic results – may be found in the Table 1. We determined zircon U/Pb (ZrnPb) dates using facilities in the Department of Earth Sciences at the University of Hong Kong; $^{40}Ar/^{39}Ar$ biotite (BtAr) and K-feldspar (KfsAr) dates using facilities at the Laboratory of Isotope Thermochronology, Institute of Geology, Chinese Academy of Geological Sciences; and (U-Th)/He zircon (ZrnHe) and apatite (ApHe) dates using facilities in the Group 18 Laboratories at Arizona State University. Detailed analytical procedures are described in the Supplementary Materials. All average dates reported and discussed below are presented with uncertainties estimated at the 2σ level.

4. Data and interpretation

Zircon U-Pb dating results are presented in Supplementary Table 1 and the concordia diagrams and the weighted dates are presented in Fig. 4. Diorite sample TS1104 yielded a weighted $^{206}Pb/^{238}U$ age of 281.9±1.2 Ma. This result suggests that the diorite was emplaced in the early Permian. The well-preserved magmatic zoning (Fig. 4a) and relatively high Th/U ratios (0.44-0.71) of TS1104 zircons suggest that the weighted mean date shows an early Permian emplacement for the diorite.

$^{40}Ar/^{39}Ar$ step-heating age spectra data for the central Tianshan samples can be found in Figs.4b-e and the Supplementary Table 2. Three biotite samples (TS1343, TS1339 and TS1104) present flat age spectra with well-defined plateaus dates accounting for more than 85% of the total-released ^{39}Ar: 312.1 ± 1.9 Ma, 293.1 ± 1.8 Ma and 239.5 ± 1.3 Ma, respectively (Figs.4b-d). K-feldspar sample TS1109 exhibits a flat age spectrum, its plateaus representing 97.3% of the total released ^{39}Ar (Fig. 4e) and indicating a date of 269.2 ± 1.4 Ma. Kfs for this sample records rapid cooling through the KfsAr closure temperature soon after the pluton emplacement.

As noted in Supplementary Tables 3 and 4, several of our samples yielded (U–Th)/He zircon and apatite age datasets that are "over-dispersed", meaning that their dispersion is greater than it would be expected from analytical imprecision alone. For example, only two samples (TS1303 and TS1341) yielded inverse-variance weighted mean ZrnHe dates that are not overdispersed (Supplementary Table 3). The remainder of the samples yielded over-dispersed (U–Th)/He results

as defined by the mean squared weighted deviation (MSWD) of each dataset (Wendt and Carl, 1991). For those datasets, we tried to identify obvious outliers using the Hampel identifier method with a threshold value of four (Pearson, 2011). For ZrnHe dating, only one date (TS1341 z003: 271.8 ± 7.8 Ma) was identified as an outlier by the Hampel identifier method. The remaining three dates ranged from 246.6 ± 7.2 Ma to 238.8 ± 6.9 Ma. After removal of the 271.8 Ma outlier date, the remaining TS1341 sample dates were not over-dispersed, with an inverse-variance weighted mean date of 242.0 ± 4.0 Ma. Three zircons from sample TS1303 were dated and not over-dispersed, with an inverse-variance weighted mean date of 125.5 ± 8.2 Ma. We also report uncertainties for the ZrnHe inverse-variance weighted mean dates of the other five over-dispersed datasets using twice the standard deviation of the population of ZrnHe dates for the sample (Supplementary Table 3). The four samples (14DK02, 14DK01, TS1343 and TS1342) yielded 102 ± 20 Ma, 172 ± 30 Ma, 230 ± 22 Ma and 243 ± 27 Ma of inverse-variance weighted mean ZrnHe dates, respectively.

All apatite (U-Th)/He dates are listed in Supplementary Table 4. Analyses TS1343 a004 and C14NL23 a006 were identified as outliers by the Hampel identifier method. After removal of these outlier dates, the remaining TS1343 and C14NL23 sample dates were still over-dispersed. As a consequence, we report uncertainties for the ApHe inverse-variance weighted mean dates of the eleven over-dispersed datasets using twice the standard deviation of the population of ApHe dates for the sample (Supplementary Table 4). The eleven samples were divided into two distinct groups. Single-grain dates of the group 1 (sample 14DK01, C14QE61, TS1342, TS1341, TS1343, TS1344 and TS1109) range from 133.1 ± 3.6 Ma to 107.8 ± 3.0 Ma, with an inverse-variance weighted mean date of 114 ± 3 Ma, 120 ± 10 Ma, 124 ± 21 Ma, 124 ± 17 Ma, 129 ± 4 Ma, 117 ± 3 and 119 ± 21 Ma, respectively. Single-grain ages of the group 2 (sample C14NL23, TS1104, 14DK02 and 14DK03) vary from 34.9 ± 1.1 Ma to 5.9 ± 1.6 Ma with an inverse-variance weighted mean date of 34.4 ± 0.8 Ma, 26.1 ± 4.7 Ma, 11.5 ± 5.2 Ma and 8.2 ± 1.5 Ma, respectively.

Only sample 14DK03 shows some positive correlation between ApHe date and effective uranium (eU) values [eU=U+0.235*Th, which is used as a proxy for a-radiation damage (Flowers et al., 2009, Fig. 5c)], indicating that the ApHe date in this sample could be influenced by radiation damage. However, the general observation exhibits no significant correlation between ApHe and ZrnHe dates and the equivalent spherical radius or the eU content for most of the apatite and zircon grains, suggests to us that the age dispersion could not be explained by grain size effects or radiation damage (Figs. 5a-b, d-e).

5. Thermal history modeling

To better understand the thermal history of our samples, thermal history modeling has been

performed using the HeFTy program (Ketcham, 2005). HeFTy input data included representative single grain ZrnHe and ApHe data. The representative grain means that its dates closes to the average date of the sample (*annotated in Supplementary Tables 3 and 4). The diffusion kinetic models used were from Farley (2000) for ApHe, and Reiners et al. (2004) for ZrnHe. BtAr and ApFT dates were manually added as constraints if available (blue boxes). All the BtAr data come from this study and the ApFT data from Dumitru et al.(2001). The closure temperatures were derived from the range of grain sizes for each mineral [biotite: 280-348 °C (Harrison et al., 1985; Grove and Harrison, 1996), ApFT: 60-110 °C (Wolf et al., 1998), ZrnHe:160-200 °C (Guenthner et al., 2013; Reiners et al., 2004), ApHe: 40-80°C (Farley, 2000), respectively]. We assume a mean surface temperature of 20±3°C at present date. The modeling started at the BtAr or the ApFT closure temperature and dates (blue box in Figs. 6c-d, g-i), or at a point 20 Ma older and 80 °C hotter than the ZrnHe thermochronometer (black box in Figs. 6a-b, e-f) to ensure successful model runs Possible cooling paths through these constraints were simulated using a Monte-Carlo approach. If a generated cooling path matched the inserted ZrnHe and ApHe data with a goodness of fit>0.05, the path was retained as a green "statistically acceptable" path. If the cooling path matched the inserted ZrnHe and ApHe data with a goodness of fit >0.5, it was retained as a purple "good fit" path. The modeling was terminated after a user-determined threshold (typically until 100 "good fits" were obtained). If no "good" fits were obtained after running one million paths, inversions were run until 100 "acceptable" fits. For each model, the best fit path and weighted mean path (weighted on GOF statistics) of all acceptable paths found are shown as black and blue curves, respectively.

Inverse modeling of ten samples suggests four episodes of cooling in the Chinese central Tianshan (Figs. 6a-i). The first episode of cooling occurred from the Late Carboniferous to early Permian (310-270 Ma) and is recorded by sample TS1109; TS1339; TS1343 (Figs. 4c-f and h). We note that this cooling episode is mainly defined by the $^{40}Ar/^{39}Ar$ age constraints and ZrnHe data from one sample (TS1344), and that the style of cooling cannot be constrained by the HeFTy modeling. The second cooling episode took place between ~245 Ma and ~210 Ma, and was found in the Baluntai town area and Dushanzi-Kuqa highway. They are recorded by $^{40}Ar/^{39}Ar$ and ZrnHe dates (TS1341, TS1342, TS1343 and C14QE61) (Table 1; Figs. 6a-c, i). The third cooling episode occurred between 140-100 Ma, as recorded by samples 14DK01, 14DK02 and TS1104 (Figs. 6d-i). The last cooling episode occurred during 30-8 Ma, as recorded by the samples TS1104, 14DK02, 14DK03 and C14NL23 (Figs. 6d, f-h).

6. *Discussion*

6.1 Late Carboniferous to early Permian exhumation history in the central Tianshan

The BtAr and KfsAr dates reported here indicate that the central Tianshan underwent profound late Carboniferous to early Permian (310-270 Ma) cooling and exhumation (Fig. 7). Also, many K-feldspar and biotite $^{40}Ar/^{39}Ar$ geochronological studies yielded a Permian cooling ages (284-267 Ma) in the Du-Ku Highway section of Chinese Tianshan (Yin et al., 1998; Zhou et al., 2001). The ZrnHe date of sample TS1344 in this study suggests a late Carboniferous cooling event. Available $^{40}Ar/^{39}Ar$ cooling dates from the main, strike-slip Tianshan shear zone also tend to cluster at this time (Laurent-Charvet et al., 2002; 2003; de Jong et al., 2009; Wang et al., 2010). The thermal history modeling results for ApFT indicates that the Western Tianshan underwent an important exhumation episode in the Early Permian (Wang et al., 2017). ApFT and ZrnHe data from the Erbin and eastern Nalati ranges indicate an early Permian (300-270 Ma) exhumation episode (Dumitru et al., 2001; Jolivet et al., 2010). The titanite fission track (TtnFT) and ZrnHe dates from the Kyrgyz South Tianshan to the west of the Nalati range also recorded the early Permian tectonic event (Glorie et al., 2011). Collectively, these results suggest that entire Tianshan may have experienced an extended period of late Carboniferous to early Permian cooling. Two main episodes of magmatism episodes have been distinguished in the Tianshan Orogen i.e. late Carboniferous and early Permian (Tang et al., 2014 and reference cited therein). Wang et al. (2006, 2007) described late Carboniferous adakite, high Mg andesite and Nb enriched arc basalt suites in the northwestern Tianshan. At the same time, many late Carboniferous mafic rocks were emplaced in the western Tianshan, e.g., the Luotuogou gabbroic pluton (312 Ma, Tang et al., 2012) and Haladala gabbroic pluton (306 Ma, Zhu et al., 2010); the Kuitui River gabbro with E-MORB compositions (302 Ma, Li et al. 2015). Li et al. (2015) proposed that widespread late Carboniferous magmatism in the western Tianshan Orogenic Belt might have been related to a ridge subduction accompanied by slab roll-back of the subducting North Tianshan Ocean plate. The Early Permian magmatic rocks consist mainly of post-collisional mafic magmatism and A-type granitic magmatism (Ma et al., 2015; Tang et al., 2014, 2017). Two alternative models have been proposed to explain the genesis of these rocks, i.e. slab break-off (Yuan et al., 2010; Ma et al., 2015; Tang et al., 2017) and mantle plume (Zhang and Zou, 2013a, b). However, Windley et al. (2007) questioned the mantle plume model and proposed that the main components of the CAOB are mostly similar to the Meso-Cenozoic circum-Pacific accretionary orogens. Yuan et al. (2010) analyzed the Permian A-type granitic rocks at Balikun and obtained zircon saturation temperatures (Tzr=841–956 °C) significantly lower than that of the A-type granites related to the Emeishan plume (Tzr=934–1053 °C) (Xu et al., 2001). Therefore, a slab break-off may explain reasonably the post-collisional magmatism and the geodynamic process of the Tianshan. We tentatively ascribe to this interpretation.

As a result, late Carboniferous to early Permian exhumation process could have been affected by a sequence of complex accretionary, subduction and collisional events in the Tianshan Orogenic Belt.

6.2 Mesozoic cooling history in the central Tianshan

6.2.1 Middle Triassic cooling history

The available thermal data, ZrnHe (sample TS1341, TS1342 and TS1343), biotite ^{40}Ar-^{39}Ar (sample TS1104) dates in this study suggest that the central Tianshan has undergone profound middle Triassic cooling and exhumation. Published ApFT dates (Dumitru et al., 2001) from the south Tianshan and the Du-Ku Highway section indicate middle Triassic cooling. Biotite $^{40}Ar/^{39}Ar$ data (samples TS1104) in this study suggests that an middle Triassic accelerated cooling may have occurred in the northern Tianshan as well. Evidence for Mesozoic exhumation is especially clear in the published apatite fission track data and thermal history modeling of Wang et al. (2017) for the western Tianshan (Chen et al., 2006, 2008; Han et al., 2008). Middle-late Triassic TtnFT and ApFT dates have been obtained for samples from the Kyrgyz Tianshan in places such as Song-kul plateau (Glorie and De Grave, 2016). Triassic cooling ages coincides with the deposition of a major alluvial conglomerate unit (ca. 215 Ma) in the adjacent Tarim Basin (Dumitru et al., 2001 and references therein) and Kuqa Basin (Jolivet et al., 2013 and references therein). Triassic cooling dates were reported within detrital apatites from Meso-Cenozoic sediments in e.g. the Chu and Ferghana basins, and the Kyrgyz Tianshan, suggesting that evidence for this episode of rapid exhumation has been preserved within the intramontane basin sediments as well (Bullen et al., 2001, 2003; De Grave et al., 2012). The Triassic event is also coeval with the onset of the so-called Cimmerian collisions on the southern Eurasian margin (De Grave et al., 2007; Glorie et al., 2010). Some authors proposed that it resulted in the reactivation of inherited Paleozoic structures in the Tianshan, Tarim and Junggar (Hendrix et al., 1992; Allen et al., 2001; De Grave et al., 2007). During the middle Triassic, the Paleo-Tethys Ocean began to close, resulting in the accretion of several Cimmerian tectonic units (e.g. Golonka, 2004). The collision/accretion of the Qiangtang block with the Kunlun terrane at the southern Eurasian margin during the middle to late Triassic coincided with Tianshan exhumation. This collision occurred along the Jinsha suture south of Tarim, in present-day Tibet and the Pamirs (e.g. Ratschbacher et al., 2003; Schwab et al., 2004; Zhai et al., 2011). It is thought that the Qiangtang collision with Eurasia induced fault reactivations and basement exhumation within Central Asia (Fig. 7). This event was suggested to be a major cause for the discordant sedimentary contact between the late Triassic and early Jurassic strata, which was discovered in the Tarim basin (Vincent and Allen, 1999). Late Triassic-early Jurassic conglomerates as well as an angular unconformity at the base of the

Jurassic are also observed at the eastern margins of the Junggar basin (Vincent and Allen, 2001). In addition, a prominent detrital zircon fission-track age peak at ~250–170 Ma supports significant Triassic–early Jurassic exhumation and unroofing of the Kunlun terranes, in northwestern Tibet (Cao et al., 2015). A palaeomagnetic study from the Chinese West Junggar demonstrates that the counter-clockwise rotations of the Junggar relative to Tarim and Siberia occurred between the early and late Triassic and were accommodated by transpressive tectonics in the Tianshan and the Altai belts (Choulet et al., 2013). This stage of exhumation and reactivation was equivalent with the Qiangtang and Kunlun-Qaidam collision, and probably resulted from the far-field effect of the collision (e.g. Hendrix et al., 1992; Dumitru et al., 2001; De Pelsmaeker et al., 2015).

Alternatively, far-field effects of the Mongol-Okhotsk Orogenic Belt to the north of the study area during the Mesozoic could also be one of the driving mechanisms for the exhumation of the Tianshan Orogen (e.g. Jolivet et al., 2010, 2013; Metelkin et al., 2010; Wilhem et al., 2012 and references therein). Johnson (2015) suggested that closure of the western Mongol-Okhotsk Ocean occurred during the Triassic. Closure of the eastern Mongol-Okhotsk Ocean may be later than its closure to the west, due in part, to a significant decrease of the magmatic activity during the late Mesozoic (Cogne et al., 2005; Donskaya et al., 2013). However, Triassic cooling is not widespread in the Siberian Altai and any relatively rapid cooling mainly occurred in the fault zones in the late Triassic (Glorie and De Grave, 2016). The timing of these events appears to be later than the middle Triassic cooling recorded in the central Tianshan. Dumitru and Hendrix (2001) investigated a syncline and faults in Mongolia and concluded that the deformation that occurred there was the result of northward thrusting. The northward orientation of thrusting suggested by Dumitru and Hendrix (2001) indicates that the driving forces for this deformation was the Cimmerian collisions to the south. Consequently, the closure of the Mongol-Okhotsk Ocean could not be responsible for the exhumation of the Chinese Tianshan in the middle Triassic.

6.2.2 Early Cretaceous cooling history

Early Cretaceous (140-100 Ma) rapid cooling was observed for the entire study area and indicates widespread exhumation throughout the Central Tianshan (Figs. 2 and 3). These Early Cretaceous ZrnHe and ApHe dates were mainly formed from the rocks in the central Tianshan or within the northern Tianshan fault zones. These dates are also similar to the data from the northern Tianshan fault zones and the Yili intramontane basin, where Dumitru et al.(2001) and Chen et al., (2008) already demonstrated the existence of early Cretaceous cooling/denudation periods using the apatite fission track method. Similar ApFT and ApHe dates have been obtained in the Kyrgyz Tianshan range (De Grave et al., 2013; Glorie and De Grave, 2016), the Chinese West Junggar (Li et al., 2014) and the Chinese Beishan (Gillespie et al., 2017). Cretaceous exhumation has been

widely recorded by ApFT analyses in the northern Tarim, southern Tianshan and adjacent regions (Dumitru et al., 2001; Sobel et al., 2006). This is consistent with some reported early Cretaceous sandstones and conglomerates in the Tarim and Junggar basins, which lie on either side of the Tianshan, and which have previously been linked to this phase of exhumation (Dumitru et al., 2001; Jolivet et al., 2010 and references therein). In addition, previous studies, which included ^{40}Ar-^{39}Ar, ApFT and ApHe dating, suggested a rapid exhumation during Cretaceous in the Eastern Kunlun (Dai et al., 2013 and references therein). The Cretaceous cooling, recorded by the thermo-chronological data in the northern Tarim, Chinese Tianshan and neighboring regions, probably resulted from far field effects of the Lhasa-Qiangtang collision at the southern Eurasian margin (De Grave et al., 2007, 2013; Dumitru et al., 2001). The distant effects of the collision propagated deformation to the interior of Eurasia and induced tectonic reactivation of the pre-existing structural fabric (Jolivet et al., 2010; De Grave et al., 2013). This could be the reason that the Early Cretaceous cooling pulse is mostly characterized by localized uplift along major strike-slip faults or the Central Tianshan block (Jolivet et al., 2010 and this study). In addition, some authors proposed that far-field effects of the MOOB to the NE of the study area during the Jurassic–Cretaceous cannot be excluded, although its extent and influence is at present highly contested (e.g. Jolivet et al., 2010, 2013; Metelkin et al., 2010; Wilhem et al., 2012 and references therein). However, the early-middle Cretaceous (130-100 Ma) cooling signal is not significant and reflects a protracted residence within the partial Annealing zone (Glorie and De Grave, 2016). The fast cooling occurred mainly during 100-90 Ma when large-scale fault reactivation took place within the Siberian Altai-Sayan. Jolivet et al. (2009) suggested that this cooling may be a tectonic response to orogenic collapse of the Mongol-Okhotsk belt. The period of compressive deformation affected a large area encompassing the northern Altai range and the whole Sayan range, but the east Tianshan and the Gobi Altai region in Mongolia are unlikely affected by this tectonic episode (Jolivet et al., 2010).

In this study, we are inclined to favor the scenario that the early Cretaceous exhumation of the Chinese Tianshan which could be caused by the Lhasa-Qiangtang collision at the southern Eurasian margin. Evidently, more work is required to understand whether the Mesozoic cooling in the Chinese Tianshan could be related to the closure of the Mongol-Okhotsk Ocean, the Qiangtang-Eurasia, even both.

6.3 Late Cenozoic cooling history in the central Tianshan

The thermal history modeling results of two samples (C14NL23 and TS1104) in the Borohoro Mts and the northern Tianshan which revealed late Eocene to late Oligocene rapid exhumation (Figs. 6e, i). The samples are located close to the north side of North Nalati Fault. Evidence for a similar ApHe dates have also been obtained in the Baluntai area (Lü et al., 2013).

Hendrix et al. (1994) found evidence for a strong tectonic reactivation during late Oligocene-early Miocene based on apatite fission track analysis from samples along the Manas river (northern Tianshan). In addition, a rapid uplift and exhumation event between 35.6-22.0 Ma has been widely reported in the Kuqa basin of the South Tianshan range with the apatite (U-Th)/He method (Yu et al., 2014). The thermal history modeling of apatite fission track length and age data show that late Oligocene-early Miocene (30-20 Ma) exhumation also occurred in the western Tianshan (Wang et al., 2017). Oligocene and Miocene cooling ages are recognized in close vicinity of major fault zones within the Kyrgyz Tianshan and Pamir (e.g. De Grave et al., 2013; Glorie and De Grave, 2015). Our data and previous studies show that rapid uplift and exhumation are recorded along the major fault zones, which are presumably linked with renewed tectonic reactivation as a far-field effect of the India-Eurasia collision (Hendrix et al., 1994; Dumitru et al., 2001; Yu et al., 2014; Glorie and De Grave, 2015). Van Hinsbergen et al. (2012) proposed that the India-Eurasia collision was divided into two periods: a 'soft' collision between Greater India and Eurasia at ～50 Ma and a 'hard' collision of India with Eurasia at ～25 Ma. The data presented here suggest that the beginning of reactivation in the Chinese Tianshan Orogen occurred during the late Eocene-late Oligocene (34.3 Ma-26.1 Ma) and thus is likely related with the 'soft' collision of India-Eurasian (Fig. 7).

The thermal history modeling results and ApHe data for two samples from the Borohoro Mountains (14DK02 and 14DK03) reveal evidence for late Miocene rapid exhumation with ApHe dates of 11.5 ± 5.2 Ma, and 8.6 ± 2.0 Ma, respectively (Table 1) and ApFT age of 15.3 Ma - 9.1 Ma (Dumitru et al., 2001; Guo et al., 2006). Both samples were collected close to the northern strand of the northern Tianshan fault. We interpret these dates as reflecting exhumation related to Cenozoic oblique slip on the fault. Yu et al. (2016) also report late Miocene ApHe dates for samples collected close to the northern Nalati Fault. Periods of rapid cooling in the late Miocene were also recorded on the southern Chinese Tianshan i.e. Kuqa fold-and-thrust belt (Yu et al., 2014; Chang et al., 2017). Accelerated exhumation at 11 Ma is indicated by magnetostratigraphy data in the northern and southern Tianshan (Charreau et al., 2006). Magnetostratigraphic and geochronologic data from the Chu Basin in the western Kyrgyz Tianshan also suggest an increase in sedimentation rate by ~11 Ma (Bullen et al., 2001; Sobel et al., 2006). In the western Tianshan, eastern Tianshan, Yili Basin and the Bayanbulak Basin, low-temperature thermochronology does not show clear evidence for such late Miocene exhumation, however few data are available. The modern Tianshan is very active seismically (Jolivet et al., 2010), with four historic earthquakes exceeding magnitude 8.0 (Ma, 1987). Based on the previous work and the data presented here, we suggest that Cenozoic deformation in the Chinese Tianshan is localized on major oblique-slip faults and is also associated with foreland folds and thrust faults in the Kuqa and Junggar Basins. Although some major shortening structures in the Tianshan have been reactivated since the early Eocene (e.g. Glorie et al., 2011), building of the modern Tianshan is generally believed to have started in the Oligocene–early Miocene, and erosional exhumation has been dominant from the

Miocene onwards (e.g. Bullen et al., 2001, 2003; De Grave et al., 2013; Jolivet et al., 2010; Sobel et al., 2006; Yu et al., 2014).

7. Conclusion

New U/Pb, $^{40}Ar/^{39}Ar$, and (U-Th)/He data and combined with thermal history modeling results provide novel insight into the tectonothermal evolution of the Chinese Tianshan. Five episodes of exhumation are apparent in the dataset.

A major exhumation episode during late Carboniferous-early Permian (310-270 Ma) is indicated by $^{40}Ar/^{39}Ar$ data from biotite and K-feldspars and zircon (U-Th)/He data for several late Devonian-early Carboniferous granitoids. This episode of exhumation may have been induced by a sequence of complex, accretionary, subduction and collisional events in the Tianshan Orogenic Belt. Other samples provide thermochronologic evidence for 245-210 Ma and 140-100 Ma exhumation, possibly caused by Cimmerian collisions at the southern Eurasian margin in the Mesozoic, which are envisaged as the main tectonic drivers of renewed Mesozoic deformational activity in the Chinese Tianshan (e.g., Jolivet et al., 2010). Finally, localized exhumation, which occurred between the late Eocene-late Oligocene and late Miocene along the northern Tianshan fault, northern Nalati Fault and subsidiary structures, is presumably related to a far-field response to the India-Eurasia collision.

Acknowledgements

This study was supported by grants from the Major Basic Research Project of the Ministry of Science and Technology of China (Grant no: 2014CB448000), the National Science Foundation of China (Grant nos. 41390441, 41473053, 41573045, 41611530698, 41703056), the China Postdoctoral Science Foundation (Grant nos. 2014M560113, 2015T80134), the China Geological Survey (Grant no. DD20160123-02) and State Key Laboratory of Isotope Geochemistry, Guangzhou Institute of Geochemistry, Chinese Academy of Sciences (Grant no. SKLabIG-KF-16-10). We thank Editor Prof. Zheng-Xiang Li and two anonymous reviewers for their critical reviews and constructive comments, which significantly improved the manuscript. We also thank Bin Zhang and Zhihua Xu for sample collection and Arnaud broussolle for his polishing of the manuscript. Many thanks to Michelle Aigner for help with lab analyses. Comments and suggestions by Prof. Fei Wang and Dr. Nathaniel Borneman on earlier versions of this manuscript are much appreciated. All analytical data presented in this study are provided in Excel format in the Supplementary Materials.

References

Allen, M. B., and Vincent, S. J., 1997. Fault reactivation in the Junggar region, northwest China: The role of basement structures during Mesozoic- Cenozoic compression, Journal of the Geological Society 154, 151-155.

Allen, M.B., Alsop, G.I., Zhemchuzhnikov, V.G., 2001. Dome and basin refolding and transpressive inversion along the Karatau fault system, southern Kazakstan. Journal of the Geological Society, Soc., London 168, 83-95.

Allen, M.B., Windley, B.F., Zhang, C., 1993. Palaeozoic collisional tectonics and magmatism of the Chinese Tien Shan, central Asia. Tectonophysics 220, 89-115.

Bullen, M. E., urbankD, W.B., Garver, J.I., 2003. Building the Northern Tien Shan: Integrated thermal, structural, and topographic constraints. Journal of geology 111, 149-165.

Bullen, M.E., Burbank, D.W., Garver, J.I., Abdrakhmatov, K.Ye, 2001. Late Cenozoic tectonic evolution of the northwestern Tien Shan: new age estimates for the initiation of mountain building. Geological Society of America Bulletin 113 (12): 1544-1559.

Buslov, M.M., Klerkx, J., Abdrakhmatov, K., Delvaux, D., Batalev, V.Y., Kuchai, O.A., Dehandschutter, B., Muraliev, A., 2003. Recent strike-slip deformation of the northern Tien Shan. In: Storti, F., Holdsworth, R.E., Salvini, F. (Eds.), Intraplate Strike-Slip Deformation Belts. Geological Society, London, Special Publications 210, 53-64.

Buslov, M.M., Saphonova, I.Yu., Watanabe, T., Obut, O.T., Fujiwara, Y., Iwata, K., Semakov, N.N., Sugai, Y., Smirnova, L.V., Kazansky, A.Yu., 2001. Evolution of the Paleo-Asian Ocean (Altai-Sayan Region, Central Asia) and collision of possible Gondwana-derived terranes with the southern marginal part of the Siberian continent. Geoscience Journal 5, 203-224.

Cao, K., Wang, G.C., Bernet, M., van der Beek, P., Zhang, K.X., 2015. Exhumation history of the West Kunlun Mountains, northwestern Tibet: Evidence for a long-lived, rejuvenated orogen. Earth and Planetary Science Letters 432, 391-403

Cassata, W.S., Renne, P.R., and Shuster, D.L., 2009. Argon diffusion in plagioclase and implications for thermochronometry: A case study from the Bushveld Complex, South Africa. Geochimica et Cosmochimica Acta 73: 6600–6612.

Chang, J., Qiu, N.S., Li, J.W., 2012. Tectono-thermal evolution of the northwestern edge of the Tarim Basin in China: Constraints from apatite (U-Th)/He thermochronology. Journal of Asian Earth Sciences 61: 187-198.

Chang, J., Tian, Y.T., Qiu, N.S., 2017. Mid-Late Miocene deformation of the northern Kuqa fold-and-thrust belt (southern Chinese Tian Shan): An apatite (U-Th-Sm)/He study. Tectonophysics 694: 101-113.

Charreau, J., Chen, Y., Gilder, S., Dominuez, S., Avouac, J.P., Sen, S., Jolivet, M., Li, Y., Wang, W., 2006. Magnetostratigraphy of the Yaha section, Tarim Basin (China), 11 Ma acceleration

in erosion and uplift of the Tian Shan mountains. Geology 34 (3), 181-184.

Chen, Z.L., Li, J., Gong, H.L., Jiang, R.B., Li, S.X., Zheng, E.J., Han, X.Z., Li, X.G., Wang, G. R., Wang, G., Lu, K.G., 2008. Preliminary study on the uplifting-exhumation process of the western Tianshan range, northwestern China. Acta Petrol. Sin. 24 (4), 625-636 (in Chinese with English abstract).

Chen, Z.L., Wan, J.L., Liu, J., Li, S.X., Zhen, E.J., Han, X.Z., Li, X.G., Gong, H.L., 2006. Multi-stage uplift and exhumation of the West Tianshan Mountain: evidence from the apatite fission track dating. Acta Geosci. Sin. 27 (2), 97-106 (in Chinese with English abstract).

Choulet, F., Chen, Y., Wang, B., Faure, M., Cluzel, D., Charvet, J., Lin, W., Xu, B., 2011. Late Paleozoic paleogeographic reconstruction of Western Central Asia based upon paleomagnetic data and its geodynamic implications. Journal of Asian Earth Sciences 42, 867-884.

Cogne, J.P., Kravchinsky, V.A., Halim, N., Hankard, F., 2005. Late Jurassic-Early Cretaceous closure of the Mongol-Okhotsk Ocean demonstrated by new Mesozoic paleomagnetic results from the Tran-Baikal area (SE Siberia). Geophysical Journal International 163, 813-832.

Dai, J.G., Wang, C.S., Hourigan, J., Santosh, M., 2013. Multi-stage tectono-magmatic events of the Eastern Kunlun Range, northern Tibet: Insights from U-Pb geochronology and (U–Th)/He thermochronology. Tectonophysics 599, 97-106.

De Grave, J., Buslov, M.M., Van den haute, P., 2007. Distant effects of India-Eurasia convergence & Mesozoic intracontinental deformation in Central Asia: constraints from apatite fission-track thermochronology. Journal of Asian Earth Sciences 29, 188-204.

De Grave, J., Glorie, S., Buslov, M.M., Izmer, A., Fournier-Carrie, A., Batalev, V.Y., Vanhaecke, F., Elburg, M.A., Van den Haute, P., 2011. The thermo-tectonic history of the Song-Kul Plateau, Kyrgyz Tien Shan: constraints by apatite and titanite thermochronometry and zircon U/Pb dating. Gondwana Research 20 (4), 745-763.

De Grave, J., Glorie, S., Buslov, M.M., Stockli, D.F., McWilliams, M.O., Batalev, Yu, V., Van den haute, P., 2013. Thermo-tectonic history of the Issyk-kul basement (Kyrgyz northern Tien Shan, Central Asia). Gondwana Research 23, 998-1020.

De Grave, J., Glorie, S., Ryabinin, A., Zhimulev, F., Buslov, M.M., Izmer, A., Elburg, M., Vanhaecke, F., Van den haute, P., 2012. Late palaeozoic and meso-Cenozoic tectonic evolution of the southern kyrgyz Tien Shan: constraints from multimethod thermochronology in the Trans-Alai, Turkestan-Alai section and the Southeastern ferghana Basin. Journal of Asian Earth Sciences 44, 149-168.

de Jong, K., Wang, B., Faure, M., Shu, L.S., Cluzel, D., Charvet, J., Ruffet, G., Chen, Y., 2009. New $^{40}Ar/^{39}Ar$ age constraints on the late Tianshan (Xinjiang, northwestern China), with emphasis on Permian fluid ingress. International Journal of Earth Sciences 98, 1239-1258.

De Pelsmaeker, E., Glorie, S., Buslov, M.M., Zhimulev, F.I., Poujol, M., Korobkin, V.V., Vanhaecke, F., Vetrov, E.V., De Grave, J., 2015. Late-Paleozoic emplacement and Meso-Cenozoic reactivation of the southern Kazakhstan granitoid basement. Tectonophysics,

662, 416-433.

Donskaya, T.V., Gladkochub, D.P., Mazukabzov, A.M., Ivanov, A.V., 2013. Late Paleozoic-Mesozoic subduction-related magmatism at the southern margin of the Siberian continent and the 150 million-year history of the Mongol-Okhosk Ocean. Journal of Asian Earth Sciences 62, 79-97.

Dumitru, T.A., Zhou, D., Chang, E.Z., Graham, S.A., 2001. Uplift, exhumation, and deformation in the Chinese Tian Shan. Geological Society of America Memoir 194, 71-99.

Enkin, R.J., Chen, Y., Courtillot, V., Besse, J., Xing, L., Zhang, Z., Zhuang, Z., Zhang, J., 1991. A Lower Cretaceous pole from South China and the Mesozoic hairpin turn of the Eurasian apparent polar wander path. Journal of Geophysical Research, Solid Earth 96, 4007-4028.

Farley, K.A., 2000. Helium diffusion from apatite: general behavior as illustrated by Durango fluorapatite. Journal of Geophysical Research: Solid Earth 105 (B2): 2903-2914.

Flowers, R.M., Ketcham, R.A., Shuster, D.L., Farley, K.A., 2009. Apatite (U-Th)/He thermochronometry using a radiation damage accumulation and annealing model. Geochimica et Cosmochimica Acta 73, 2347-2365.

Gao, J., Li, M., Xiao, X., Tang, Y., He, G., 1998. Paleozoic tectonic evolution of the Tianshan orogen, northwestern China. Tectonophysics 287, 213–231.

Gao, J., Long, L.L., Klemd, R., Qian, Q., Liu, D.Y., Xiong, X.M., Su, W., W.L., Wang, Y.T., Yang, F.Q., 2009. Tectonic evolution of the Southern Tianshan orogen, NW China: geochemical and age constraints of granitoid rocks. International Journal of Earth Sciences 98, 1221–1238.

Gillespie, J., Glorie, S., Xiao, W.J., Zhang, Z.Y., Collins, A.S., Evans, N., McInnes, B., De Grave, J., 2017. Mesozoic reactivation of the Beishan, southern Central Asian Orogenic Belt: Insights from low-temperature thermochronology. Gondwana Research 43, 107-122.

Glorie, S., De Grave, J., Buslov, M.M., Elburg, M.A., Stockli, D.F., Gerdes, A., Van den Haute, P., 2010. Multi-method chronometric constraints on the evolution of the Northern Kyrgyz Tien Shan granitoids (Central Asian Orogenic Belt): from emplacement to exhumation. Journal of Asian Earth Sciences 38 (3-4), 131-146.

Glorie, S., De Grave, J., Buslov, M.M., Zhimulev, F.I., Stockli, D.F., Batalev, V.Y., Izmer, A., Van den haute, P., Vanhaecke, F., Elburg, M., 2011. Tectonic history of the Kyrgyz South Tien Shan (Atbashi-Inylchek) suture zone: the role of inherited structures during deformation-propagation. Tectonics 30, TC6016 1-23.

Glorie, S., De Grave.J., 2015. Exhuming the Meso–Cenozoic Kyrgyz Tianshan and Siberian Altai-Sayan: A review based on low-temperature thermochronology. Geoscience Frontiers, 7(2): 155-170.

Golonka, J., 2004. Plate tectonic evolution of the southern margin of Eurasia in the Mesozoic and Cenozoic. Tectonophysics 381, 235-273.

Guenthner, W.R., Reiners, P.W., Ketcham, R.A., Nasdala, L., Giester, G., 2013. Helium diffusion in natural zircon: radiation damage, anisotropy, and the interpretation of zircon (U-Th)/He

thermochronology. American Journal of Science 313 (3):145-198.

Han, X.Z., Cai, Y.Q., Zheng, E.J., Chen, Z.L., Zhang, Z.L., Liu, Q., 2008. Uplift-denudation in the south margin and its sedimentary response in the southern Yili basin: analysis apatite fission track method. Acta Petrol. Sin. 24 (10), 2447-2455 (in Chinese with English abstract).

Harrison, T.M., Duncan, I., McDougall, I., 1985. Diffusion of ^{40}Ar in biotite: temperature, pressure and compositional effects. Geochimica et Cosmochimica Acta 49 (11): 2461-2468.

Hendrix, M.S., Dumitru, T.A., Graham, S.A., 1994. Late Oligocene-Early Miocene unroofing in the Chinese Tien Shan-an early effect of the India-Asian collision. Geology 22, 487-490.

Hendrix, M.S., Graham, S.A., Carroll, A.R., Sobel, E.R., McKnight, C.L., Schulein, B.J., Wang, Z., 1992. Sedimentary record and climatic implications of recurrent deformation in the Tien Shan: evidence from Mesozoic strata of the north Tarim, south Junggar, and Turpan basins, Northwest China. Geological Society of America Bulletin 104 (1): 53-79.

Hodges, K. V., 2014. Thermochronology in Orogenic Systems, in Treatise on Geochemistry, Volume 3: The Crust, edited by R. L. Rudnick, pp. 281-308, Elsevier Science, Amsterdam

Jahn, B.M., Wu, F., Chen, B., 2000. Massive granitoid generation in Central Asian: Nd isotope evidence and implication for continental growth in the Phanerozoic. Episodes 23, 82–92.

Johnson, C.L., 2015. Sedimentary basins in transition: distribution tectonic settings of Mesozoic strata in Mongolia. In: Anderson, T.H., Didenko, A.N., Johnson, C.L., Khancuk, A.I., MacDonald, J.H. (Eds.), Late Jurassic Margin-A Record of Faulting Accommodating Plate Rotation, Geological Society America Special Paper 513, 543-560.

Jolivet, M., Brunel, M., Seward, D., Xu, Z., Yang, J., Roger, F., Malavieille, Tapponnier, J., Arnaud, N., Wu, C., 2001. Mesozoic and Cenozoic tectonic of the northern edge of the Tibetan plateau: fission track constraints. Tectonophysics 343, 111-134.

Jolivet, M., De Boisgrollier, T., Petit, C., Fournier, M., Sankov, V.A., Ringenbach, J.-C., Byzov, L., Miroshnichenko, A.I., Kovalenko, S.N., Anisimova, S.V., 2009. How old is the Baikal Rift Zone? Insight from apatite fission track thermochronology. Tectonics 28, TC3008.

Jolivet, M., Dominguez, S., Charreau, J., Chen, Y., Li, Y.G., Wang, Q.C., 2010. Mesozoic and Cenozoic tectonic history of the central Chinese Tian Shan: reactivated tectonic structures and active deformation. Tectonics 29, TC6019.

Jolivet, M., Heilbronn, G., Robin, C., Barrier, L., Bourquin, S., Guo, Z., Jia, Y., Guerit, L., Yang, W., Fu, B., 2013. Reconstructing the Late Palaeozoic e Mesozoic topographic evolution of the Chinese Tian Shan: available data and remaining uncertainties. Advances in Geosciences 37, 7-18.

Kapp, P., DeCelles, P.G., Gehrels, G.E., Heizler, M., Ding, L., 2007. Geological records of the Lhasa-Qiangtang and Indo-Asian collisions in the Nima area of central Tibet. Geological Society of America Bulletin 119, 917-932.

Kapp, P., Murphy, M.A., Yin, A., Harrison, T.M., Ding, L., Guo, J., 2003. Mesozoic and Cenozoic tectonic evolution of the Shiquanhe area of western Tibet. Tectonics 22, 1029.

Ketcham, R.A., 2005. Forward and inverse modeling of low-temperature thermochronometry data. Reviews in Mineralogy and Geochemistry 58 (1): 275-314.

Laurent-Charvet, S., Charvet, J., Monié, P., Shu, L.S., 2003. Late Paleozoic strike- slip shear zones in eastern Central Asia (NW China): New structural and geochronological data. Tectonics 22(2), 1009.

Laurent-Charvet, S., Charvet, J., Shu, L.S., Ma, R.S., Lu, H.F., 2002. Paleozoic late collisional strike-slip deformation in Tinshan and Altay, eastern Xinjiang, NW China. Terra Nova 14, 249-256.

Li, C., Xiao, W.J., Han, C.M., Zhou, K.F., Zhang, J.E., and Zhang, Z.X., 2015. Late devonian–early permian accretionary orogenesis along the North Tianshan in the southern Central Asian Orogenic Belt: International Geology Review 57, 1023–1050.

Li, G.M., Cao, M.J., Qin, K.Z., Evans, N.J., McInnes, B.I.A., Liu, Y.S., 2014. Thermal-tectonic history of the Baogutu porphyry Cu deposit, West Junggar as constrained from zircon U-Pb, biotite Ar/Ar and zircon/apatite (U-Th)/He dating. Journal of Asian Earth Sciences 79, 741-758.

Lü, H.H, Chang, Y., Wang, W., Zhou, Z.Y., 2013. Rapid exhumation of the Tianshan Mountains since the early Miocene: Evidence from combined apatite fission track and (U-Th)/He thermochronology. Science China: Earth Sciences 43, 1964-1974.

Ma, X., 1986. Lithospheric dynamic map of China and adjacent seas with explanatory notes, scale 1/4,000,000, Geological Publishing House.

Ma, X.X., Shu, L.S., Meert, J.G., 2015. Early Permian slab breakoff in the Chinese Tianshan belt inferred from the post-collisional granitoids. Gondwana Research, 27(1), 228-243.

Metcalfe, I., 2013. Gondwana dispersion and Asian accretion: tectonic and palaeogeographic evolution of eastern Tethys. Journal of Asian Earth Sciences 66, 1-33.

Metelkin, D.V., Vernikovsky, V.A., Kazansky, A.Y., Wingate, M.T.D., 2010. Late Mesozoic tectonics of Central Asia based on paleomagnetic evidence. Gondwana Research 18, 400-419.

Metelkin, D.V., Vernikovsky, V.A., Kazansky, A.Yu., 2012. Tectonic evolution of the Siberian paleocontinent from the Neoproterozoic to the Late Mesozoic: paleomagnetic record and reconstructions. Russian Geology and Geophysics 53, 675-688.

Pearson, R.K., 2011. Exploring Data in Engineering, the Sciences, and Medicine. Ox-ford University Press.

Qiu, N.S., Jiang, G., Mei, Q.H., Chang, J., Wang, S.J., and Wang, J.Y., 2011. The Paleozoic tectonothermal evolution of the Bachu Uplift of the Tarim Basin, NW China: Constraints from (U-Th)/He ages, apatite fission track and vitrinite reflectance data. Journal of Asian Earth Sciences 41, 551-563.

Ratschbacher, L., Hacker, B.R., Webb, L.E., Grimmer, J.C., McWilliams, M.O., Ireland, T., Dong, S., Hu, J.M., 2003. Tectonics of the Qinling (Central China): tectonostratigraphy,

geochronology, and deformation history. Tectonophysics 366, 1-53.

Reiners, P.W., Spell, T.L., Nicolescu, S., Zanetti, K.A., 2004. Zircon (U-Th)/He thermochronometry: He diffusion and comparisons with $^{40}Ar/^{39}Ar$ dating. Geochimica et Cosmochimica Acta 68(8): 1857-1887.

Roger, F., Jolivet, M., Malavieille, J., 2010. The tectonic evolution of the Songpan-Garzê (North Tibet) and adjacent areas from Proterozoic to Present: a synthesis. Journal of Asian Earth Sciences 39, 254-269.

Schwab, M., Ratschbacher, L., Siebel, W., McWilliams, M., Minaev, V., Lutkov, V., Chen, F., Stanek, K., Nelson, B., Frisch, F., Wooden, J.L., 2004. Assembly of the Pamirs: age and origin of magmatic belts from the southern Tien Shan to the southern Pamirs and their relation to Tibet. Tectonics 23, 31.

Sobel, E.R., Chen, J., Heermance, R.V., 2006. Late Oligocene-Early Miocene initiation of shortening in the Southwestern Chinese Tian: implications for Neogene shortening rate variations. Earth and Planetary Science Letters 247 (1-2), 70-81.

Sobel, E.R., Dumitru, T.A., 1997. Thrusting and exhumation around the margins of the western Tarim basin during the India-Asia collision. Journal of Geophysical Research 102, 5043-5063.

Sun, J.M., Zhu, R.X., James, B., 2004. Timing of the Tian Shan Mountains uplift constrained by magnetostratigraphic analysis of molasses deposits. Earth and Planetary Science Letters 219: 239-253.

Tang, G.J., Wang, Q., Wyman, D.A., Li, Z.X., Xu, Y.G., Zhao, Z.H., 2012. Metasomatized lithosphere-asthenosphere interaction during slab roll-back: evidence from Late Carboniferous gabbros in the Luotuogou area, Central Tianshan. Lithos 155, 67-80.

Tang, G.J., Chung, S.L., Wang, Q., Wyman, D.A., Dan, W., Chen, H.Y., Zhao, Z.H., 2014. Petrogenesis of a Late Carboniferous mafic dike–granitoid association in the western Tianshan: Response to the geodynamics of oceanic subduction, Lithos, 202-203, 85-99.

Tang, G.J., Cawood, P.A., Wyman, D.A., Wang, Q., Zhao, Z.H., 2017. Evolving mantle sources in post-collisional early Permian-Triassic magmatic rocks in the heart of Tianshan Orogen (western China). Geochemistry, Geophysics, Geosystems, DOI:10.1002/2017GC006977.

Van Hinsbergen, D.J.J., Lippert, P.C., Dupont-Nivet, G., McQuarrie, N., Doubrovine, P.V., Spakman, W., Torsvik, T.H., 2012. Greater India Basin hypothesis and a two-stage Cenozoic collision between India and Asia. Proceedings of the National Academy of Sciences of the United States of America 109, 7659-7664.

Vincent, S.J., Allen, M.B., 1999. Evolution of the Minle and Chaoshui Basins, China: implications for Mesozoic strike-slip basin formation in Central Asia. Geological Society of America bulletin 111, 725-742.

Vincent, S.J., Allen, M.B., 2001. Sedimentary record of Mesozoic intracontinental deformation in the eastern Junggar Basin, northwest China: Response to orogeny at the Asian margin.

Geological Society of America Memoir 194, 341-360.

Wagner, G.A., Gleadow, A.J.W., Fitzgerald, P.G., 1989. The significance of the partial annealing zone in apatite fission-track analysis: Projected track length measurements and uplift chronology of the transantarctic mountains. Chemical Geology 79, 295-305.

Wang, B., Faure, M., Shu, L.S., de Jong, K., Charvet, J., Cluzel, D., Jahn, B., Chen, Y., Ruffet, G., 2010. Structural and geochronogical study of high-pressure metamorphic rocks in the Kekesu section (northwestern China): implications for the late Paleozoic tectonics of the Southern Tianshan. Journal of Geology 118, 59-77.

Wang, Q., Li, S., Du, Z., 2009. Differential uplift of the Chinese Tianshan since the Cretaceous: constraints from sedimentary petrography and apatite fission-track dating. International Journal of Earth Sciences 98, 1341-1363.

Wang, Q.,Wyman, D.A., Zhao, Z.H., Xu, J.F., Bai, Z.H., Xiong, X.L., Dai, T.M., Li, C.F., Chu, Z.Y., 2007. Petrogenesis of Carboniferous adakites and Nb-enriched arc basalts in the Alataw area, northern Tianshan Range (western China): implications for Phanerozoic crustal growth in the Central Asia orogenic belt. Chemical Geology 236 (1–2), 42–64.

Wang, Q., Zhao, Z.H., Xu, J.F., Wyman, D.A., Xiong, X.L., Zi, F., Bai, Z.H., 2006. Carboniferous adakite-high-Mg andesite-Nb-enriched basaltic rock suites in the Northern Tianshan area: Implications for Phanerozoic crustal growth in the Central Asia Orogenic Belt and Cu-Au mineralization. Acta Petrologica Sinica 22 (1), 11–30 (in Chinese with English abstract).

Wang, Y.N., Cai, K.D., Sun, M., Xiao, W.J., De Grave, J., Wan, B., Bao, Z.H., 2017. Tracking the multi-stage exhumation history of the western Chinese Tianshan by apatite fission track (AFT) dating: Implication for the preservation of epithermal deposits in the ancient orogenic belt. Ore Geology Reviews, doi.org/10.1016/j.oregeorev.2017.04.011

Wendt, I., Carl, C., 1991. The statistical distribution of the mean squared weighted deviation. Chemical Geology: Isotope Geoscience Section 86, 275–285.

Wilhem, C., Windley, B.F., Stampfli, G.M., 2012. The Altaids of Central Asia: a tectonic and evolutionary innovative review. Earth-Science Reviews 113, 303-341.

Windley, B.F., Alexeiev, D., Xiao, W., Kröner, A., Badarch, G., 2007. Tectonic models for accretion of the Central Asian Orogenic Belt. Journal of the Geological Society, London 164, 31–47.

Windley, B.F., Allen, M.B., Zhang, C., Zhao, Z.Y., Wang, G.R., 1990. Paleozoic accretion and Cenozoic redeformation of the Chinese Tien Shan Range, Central Asia. Geology 18, 128-131.

Wolf, R.A., Farley, K.A., Kass, D.M., 1998. Modelling of the temperature sensitivity of the apatite (U-Th)/He thermochronometer. Chemical Geology 148: 105-114.

Xiao, W.J., Han, C.M., Yuan, C., Sun, M., Lin, S.F., Chen, H.L., Li, Z.L., Li, J.L., Sun, S., 2008. Middle Cambrian to Permian subduction–related accretionary orogenesis of North Xinjiang, NW China: implications for the tectonic evolution of Central Asia. Journal of Asian Earth

Sciences 32, 102–117.

Xiao, W.J., Santosh, M., 2014. The western Central Asian Orogenic Belt: A window to accretionary orogenesis and continental growth. Gondwana Research 25, 1429-1444.

Xiao, W.J., Windley, B.F., Allen, M., Han, C.M., 2013. Paleozoic multiple ccretionary and collisional tectonics of the Chinese Tianshan orogenic collage. Gondwana Research 23, 1316–1341.

Xiao, W.J., Windley, B.F., Yuan, C., Sun, M., Han, C.M., Lin, S.F., Chen, H.L., Yan, Q.R., Liu, D.Y., Qin, K.Z., Li, J.L., Sun, S., 2009. Paleozoic multiple subduction–accretion processes of the southern Altaids. American Journal of Science 309, 221–270.

Xu, Y.G., Chung, S.L., Jahn, B.M., Wu, G.Y., 2001. Petrologic and geochemical constraints on the petrogenesis of Permian–Triassic Emeishan flood basalts in southwestern China. Lithos 58, 145-168.

Yang, Y.T., Guo, Z.X., Song, C.C., Li, X.B., He, S., 2015. A short but significant Mongol-Okhotsk collisional orogeny in latest Jurassic-earliest Cretaceous. Gondwana Research 28 (3), 1096-1116.

Yin, A., Nie, S., Craig, P., Harrison, T.M., Ryerson, F., Qian, X., Yang, G., 1998. Late Cenozoic tectonic evolution of the southern Chinese Tian Shan. Tectonics 17, 1-27.

Yin, J.Y., Chen, W., Xiao, W.J., Yuan, C., Zhang, B., Cai, K.D., Long, X.P., 2017. Petrogenesis of Early Carboniferous adakitic dikes, Sawur region, northern West Junggar, NW China: Implications for geodynamic evolution. Gondwana Research 27(4): 1630-1645.

Yu, S., Chen, W., Evans, N.J., McInnes, B.I.A., Yin, J., Sun, J., Li, J., Zhang, B., 2014. Cenozoic uplift, exhumation and deformation in the north Kuqa Depression, China as constrained by (U-Th)/He thermochronometry. Tectonophysics 630, 166-182.

Yu, S., Chen, W., Zhang, B., Sun, J.B., Li, C., Yuan, X., Shen, Z., Yang, L., Ma, X., 2016. Mesozoic and Cenozoic uplift and exhumation history of the Kekesu section in the Center Tianshan: constrained from (U-Th)/He thermochronometry. Chinese Journal of Geophysics. 59(8): 2922-2936 (in Chinese with English abstract).

Yuan, C., Sun, M., Wilde, S., Xiao,W.J., Xu, Y.G., Long, X.P., Zhao, G.C., 2010. Post-collisional plutonsin the Balikun area, East Chinese Tianshan: evolvingmagmatismin response to extension and slab break-off. Lithos 119, 269-288.

Zhai, Q.G., Jahn, B.M., Zhang, R.Y., Wang, J., Su, L., 2011. Triassic subduction of the Paleo-Tethys in northern Tibet, China: evidence from the geochemical and isotopic characteristics of eclogites and blueschists of the Qiangtang block. Journal of Asian Earth Sciences 42, 1356-1370.

Zhang, Z., Zhu, W., Shu, L., Wan, J., Yang, W., Su, J., and ZrHeng, B., 2009. Apatite fission track thermochronology of the Precambrian Aksu blueschist, NW China: Implications for thermo-tectonic evolution of the north Tarim basement. Gondwana Research 16, 182-188.

Zhang, C.L., Zou, H.B, 2013a. Permian A-type granites in Tarim and western part of Central

Asian Orogenic Belt (CAOB): genetically related to a common Permian mantle plume? Lithos, 172-173, 47-60.

Zhang, C.L., Zou, H.B, 2013b. Comparison between the Permian mafic dykes in Tarim and the western part of Central Asian Orogenic Belt (CAOB), NW China: Implications for two mantle domains of the Permian Tarim Large Igneous Province. Lithos, 174, 15-27.

Zhou, D., Graham, S.A., Chang, E.Z., Wang, B., Bradley, H., 2001. Paleozoic amalgamation of the Chinese Tian Shan: evidence from a transect along the Dushanzi-Kuqa Highway. In: Hendrix, M.S., Davis, G.A. (Eds.), Paleozoic and Mesozoic Tectonic Evolution of Central and Eastern Asia: From Continental Assembly to Intracontinental Deformation. Geological Society of America Memoir 194, 23-46.

Zhu, Y.F., Zhang, L.F., Gu, L.B., Guo, X., Zhou, J.B., 2005. The zircon SHRIMP chronology and trace element geochemistry of the Carboniferous volcanic rocks in western Tianshan Mountains. Chinese Science Bulletin 50, 2201-2212.

Table 1 Summary of sample localities and zircon U-Pb ages and thermochronological data in the Chinese central Tianshan

Supplementary Table 1 LA-ICP–MS U-Pb isotopic analysis for zircons from the diorite in the Chinese Tianshan.

Supplementary Table 2 ^{40}Ar-^{39}Ar step-heating dating results of the granitiods in the Chinese central Tianshan.

Supplementary Table 3 Individual zircon (U-Th)/He results from the Chinese central Tianshan.

Supplementary Table 4 Individual apatite (U-Th)/He results from the Chinese central Tianshan.

Fig. 1. (a) Tectonic sketch map of Central Asia (modified after Enkin et al., 1991); (b) General topographic and tectonic map of the Tianshan. The position and nature of the fault are drawn from Jolivet et al. (2010). The broken black square corresponds to the study area detailed in Figs 2 and 3. STS-Southern Tianshan; CTS-Central Tianshan; NTS-Northern Tianshan; Nalati F-Nalati Fault; NTSF-Northern Tianshan Fault.

Fig 2. Geologic map of Dushanzi-Kuqa Highway corridor across Tianshan with ApHe and ZrHe data and sample localities (modified after Dumitru et al.(2001)); ApHe data of TS1370 and TS1371 is from Yu et al.(2016); ApFT data of DK27 and DK28 is from Dumitru et al.(2001). See supplementary Tables 3 and 4 for detailed data.

Fig.3. Geological map of Baluntai area in the central Tianshan range (after Yin et al., 2017). Thermochronological data from this study is indicated with the corresponding coordinates. See supplementary Tables 3 and 4 for detailed data.

Fig.4. Zircon U-Pb concordia diagrams for sample TS1104 and biotite and K-feldspars, plagioclase $^{40}Ar/^{39}Ar$ release spectra for samples TS1104, TS1109, TS1339 and TS1343. See supplementary Tables 1 and 2 for detailed data.

Fig. 5. (a) ApHe age versus equivalent spherical radius. (b-c) ApHe age versus eU (effective U concentration: U + 0.235*Th). Sample 14DK03 displays positive correlation between ApHe age and eU. (d) ZrnHe age versus eU; (e) ZrnHe age versus equivalent spherical radius. The errors plotted are 2-sigma standard deviation.

Fig. 6 Results of thermal history modeling of selected samples from the central Tianshan. GOF=goodness-of-fit. ZrnHe=zircon (U-Th)/He. ApHe=apatite (U-Th)/He. The best fit path and weighted mean path are shown as black and blue curves, respectively.

Fig. 7 Interpreted thermal and geological history of the central Tianshan derived from the data and modeling. The data of BtAr, KfsAr, ZrnHe and ApHe is from Tables 1 and supplementary Tables 3 and 4. The best-fit paths of modeling shown in Fig. 7 were extracted from Fig. 6. The main tectonic events closely associated to the thermal and geological in the Chinese Tianshan are derived from the following references: Qiangtang and Kunlun-Qaidam collision (Ratschbacher et al., 2003; Schwab et al., 2004; Zhai et al., 2011; Glorie and De Grave, 2016); Qiangtang-Lhasa collision (Kapp et al., 2007); Karakoram-Eurasia collision (Schwab et al., 2004); India-Asia “soft” collision and India-Asia “hard” collision (Van Hinsbergen et al., 2012); Mongol-Okhotsk Orogen initiation (Metelkin et al., 2010); Mongol-Okhotsk Orogeny (Yang et al., 2015). C =Carboniferous, P =Permian, T =Triassic, J =Jurassic, K =Cretaceous, Pa =Paleogene, N =Neogene.

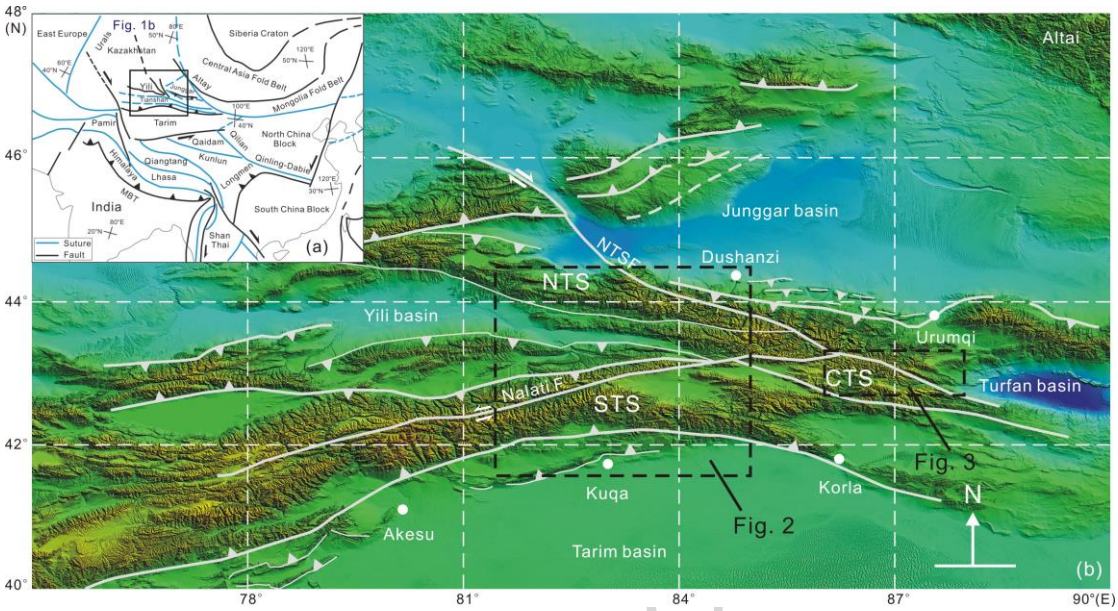

Fig. 1

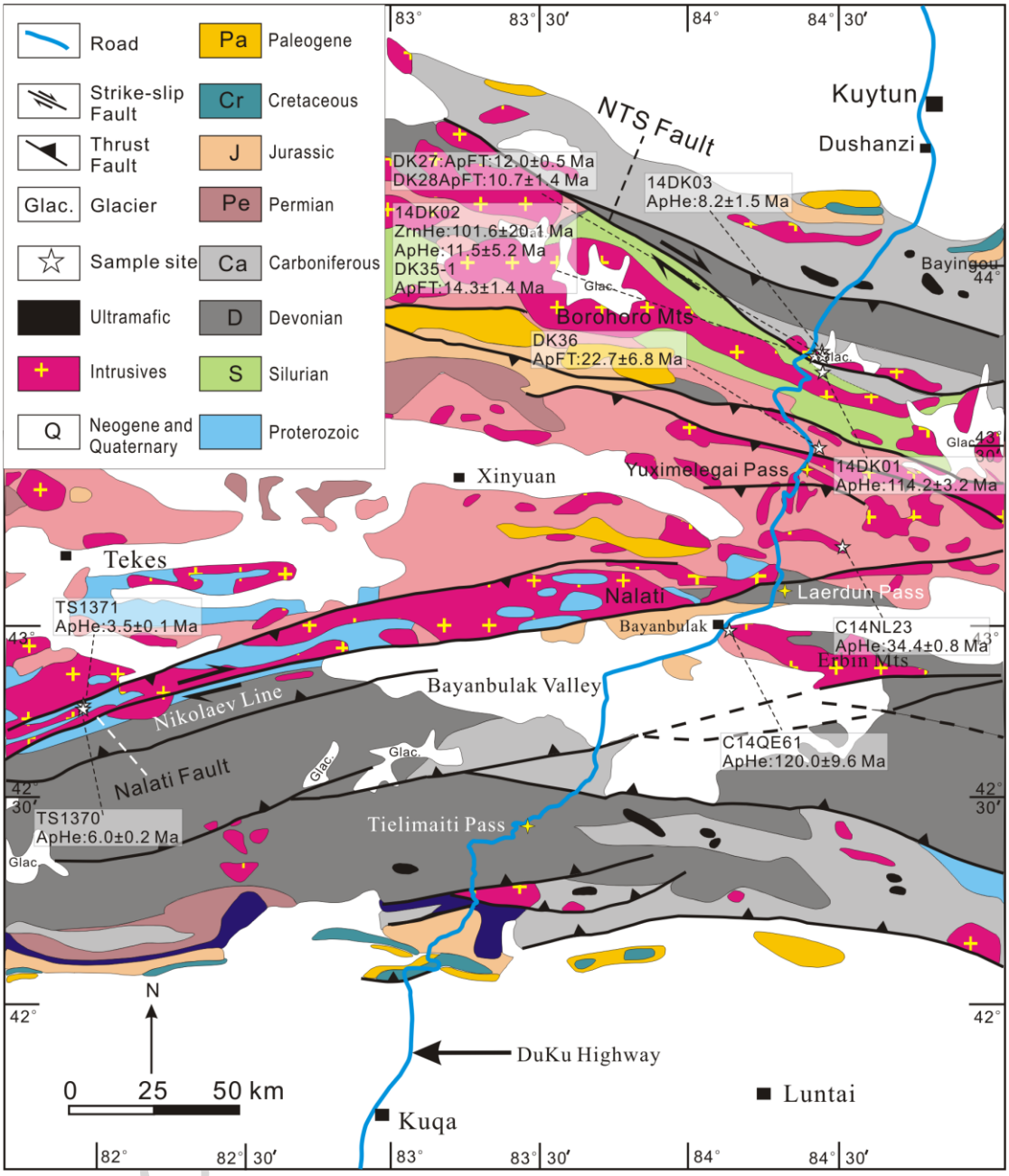

Fig. 2

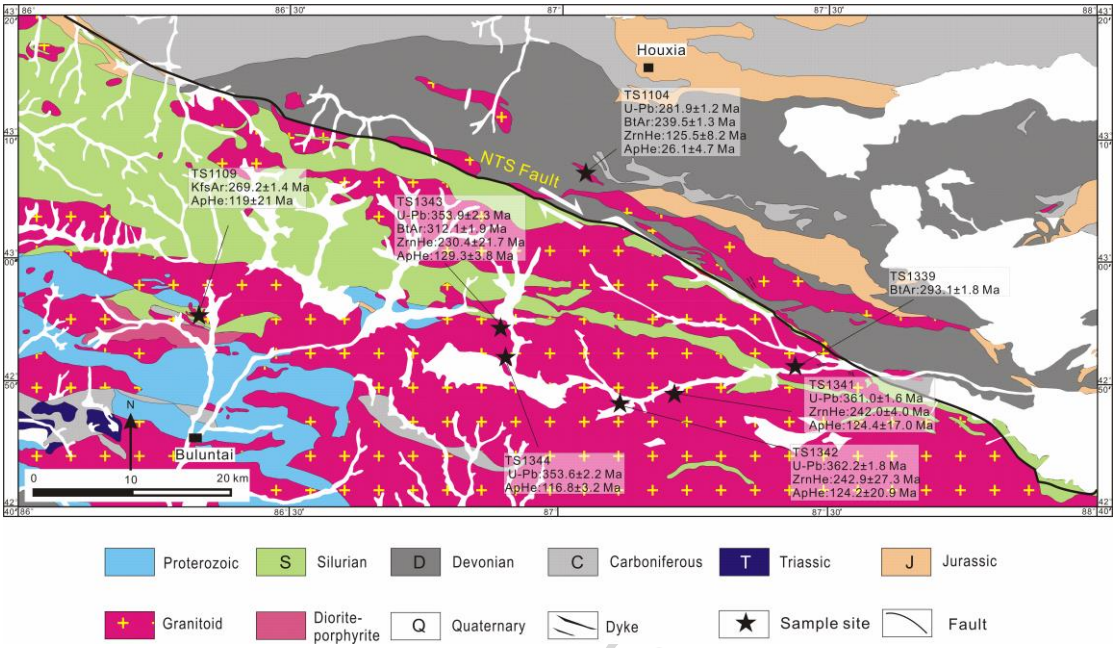

Fig. 3

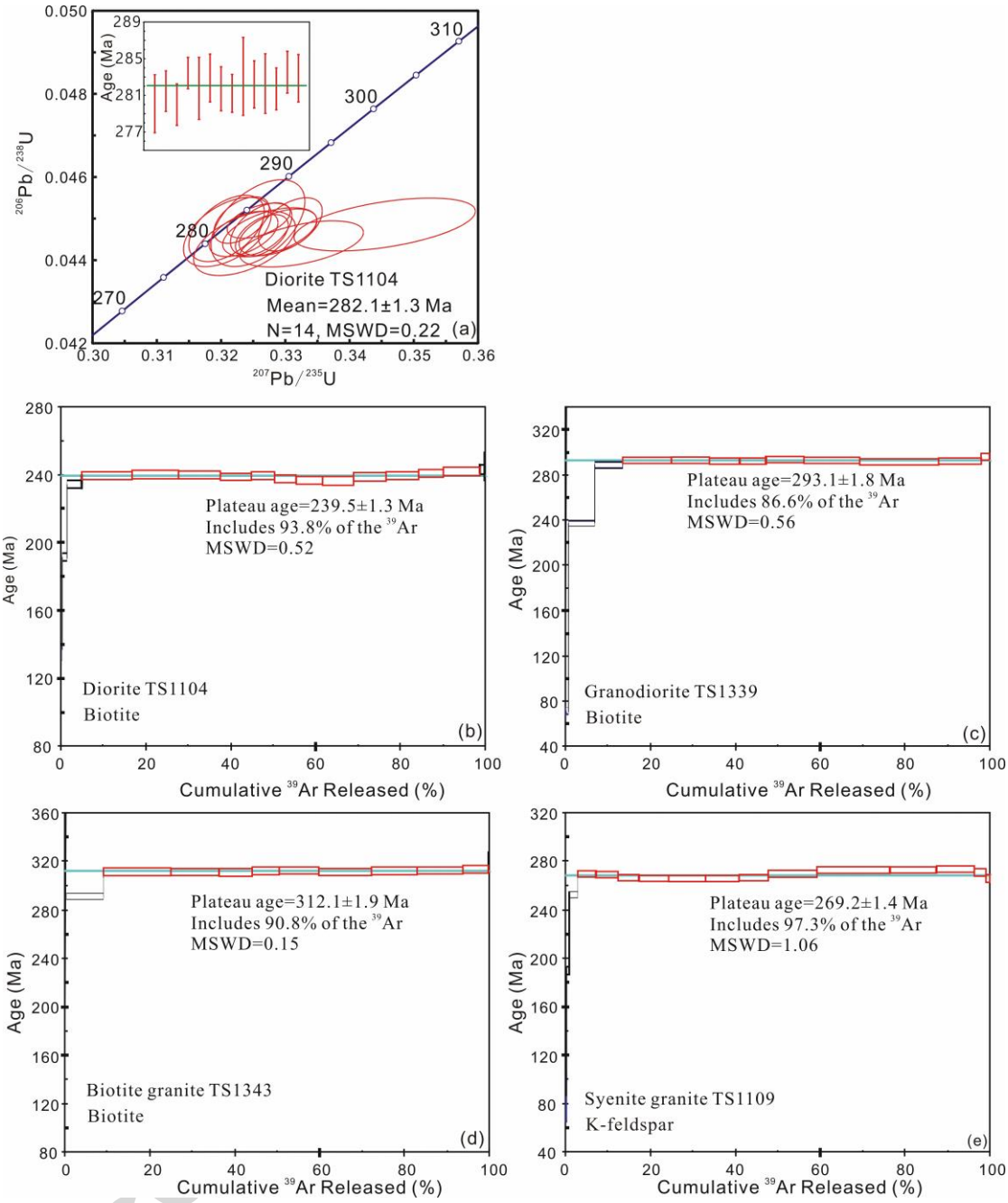

Fig. 4

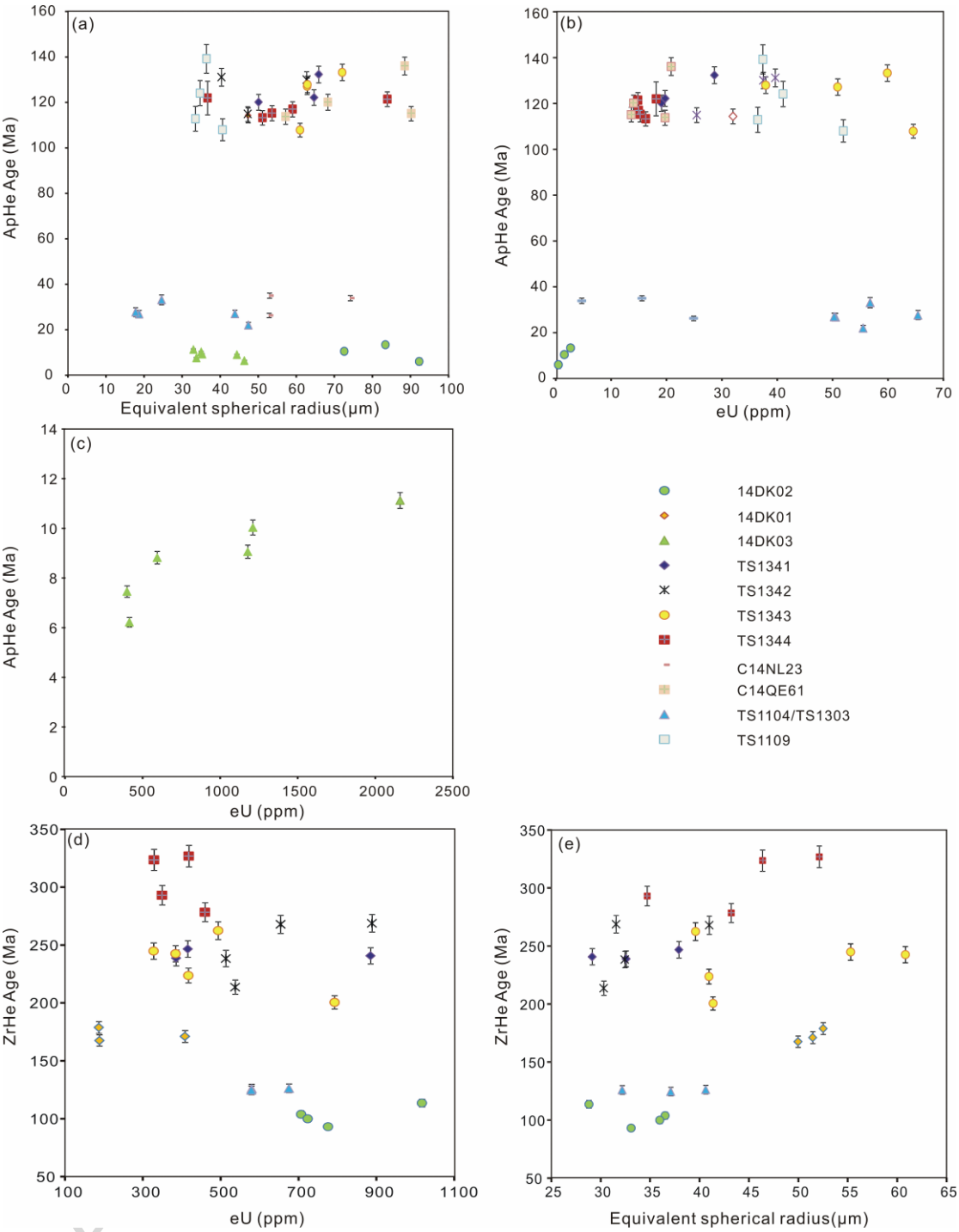

Fig. 5

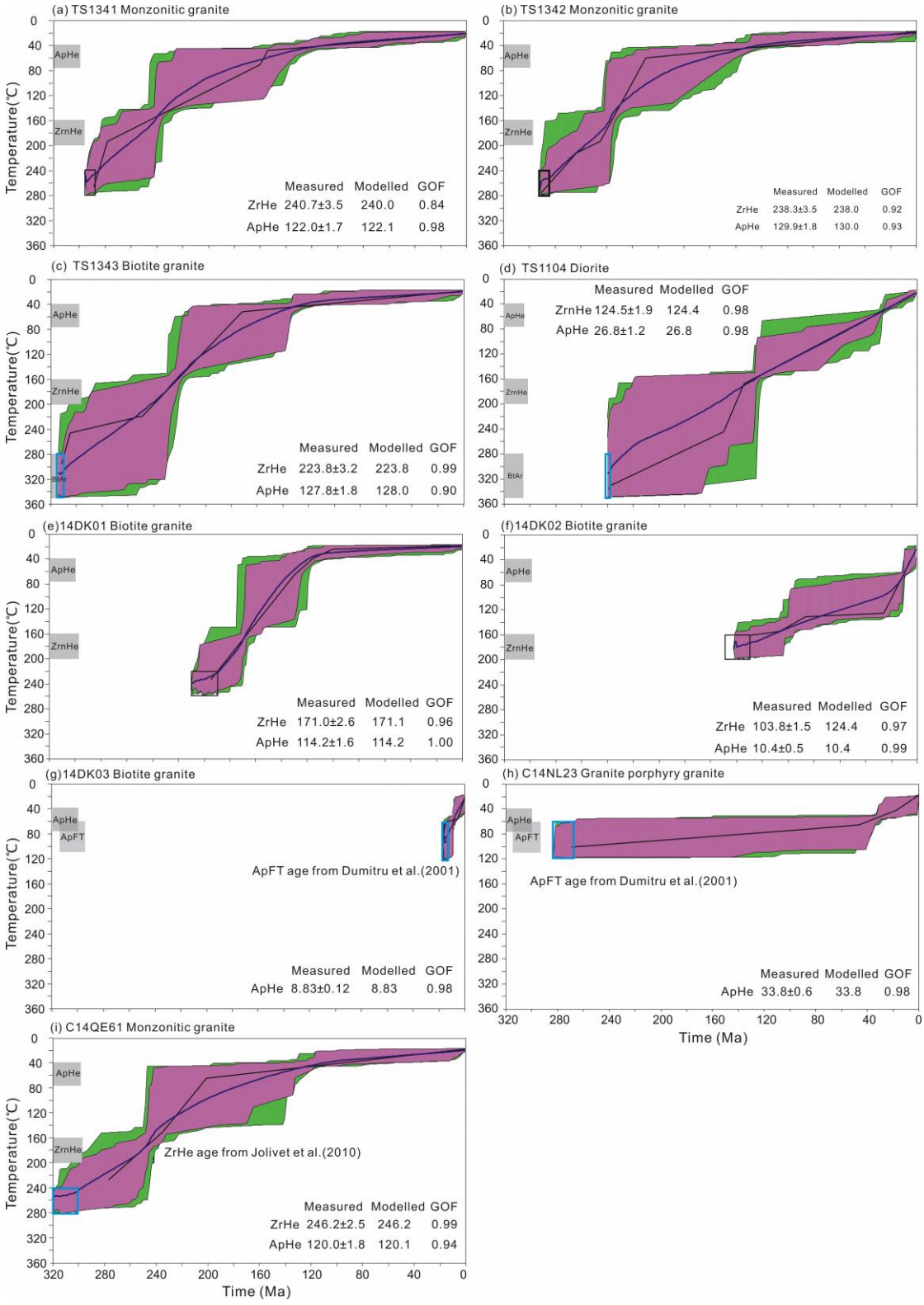

Fig. 6

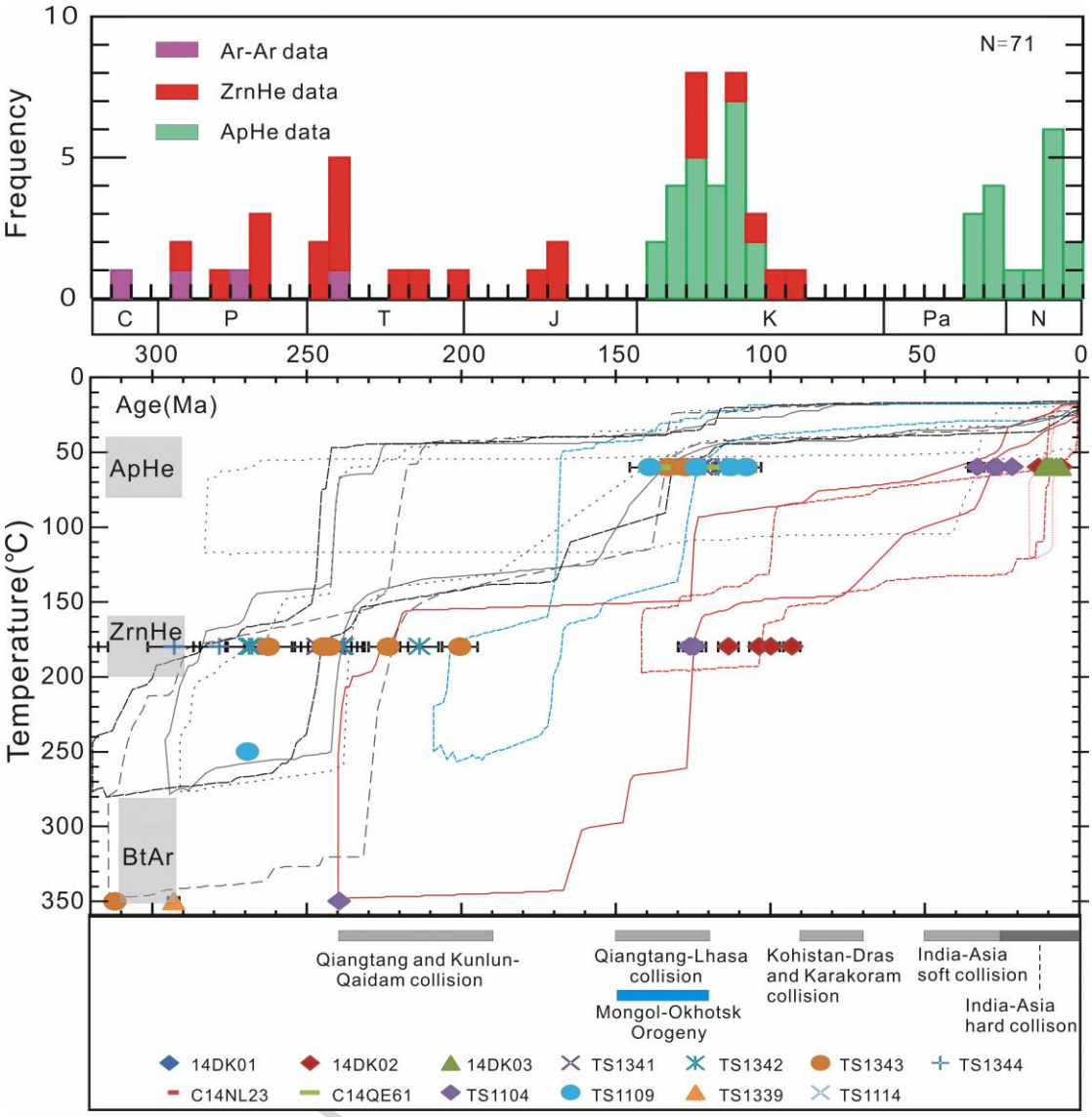

Fig. 7

Table 1 Summary of sample localities and zircon U-Pb ages and thermochronological data in the Chinese central Tianshan

Samples	Elevation (m)	GPS position	Lithology	Zircon U-Pb (Ma)	BtAr (Ma)	KfsAr (Ma)	ZrnHe (Ma)	ApHe (Ma)
14DK01	3119	43º42'22.3"N, 84º27'10.3"E	Biotite granite					114.2 ± 3.2
14DK02	3248	43º44'37.1"N, 84º25'18.8"E	Biotite granite				101.6 ± 20.1	11.5 ± 5.2
14DK03	2784	43º46'40.2"N, 84º27'18.7"E	Biotite granite					8.2 ± 1.5
C14NL23	1883	43º16'01"N, 84º31'02"E	Granite-porphyry					34.4 ± 0.8
C14QE61	2440	43º01'43"N, 84º08'34"E	Monzonitic granite					120.0 ± 9.6
TS1341	2252	42º49'32"N, 87º12'32"E	Monzonitic granite	361.0 ± 1.6*			242.0 ± 4.0	124.4 ± 17.0
TS1342	2395	42º48'35"N, 87º07'19"E	Monzonitic granite	362.2 ± 1.8*			242.9 ± 27.3	124.2 ± 20.9
TS1343	3177	42º54'22"N, 86º54'02"E	Biotite granite	353.9 ± 2.3*	312.1 ± 1.9		230.4 ± 21.7	129.3 ± 3.8
TS1344	2965	42º52'09"N, 86º54'22"E	Biotite granite	353.6 ± 2.2*			303.3 ± 23.7	116.8 ± 3.2
TS1303/TS1104	2563	43º06'58"N, 87º02'24"E	Diorite	281.9±1.2	239.5 ± 1.3		125.5 ± 8.2	26.1 ± 4.7
TS1109	2589	42º55'10"N, 86º10'42"E	Syenite granite			269.2 ± 1.4		119 ± 21
TS1339	1749	42º51'05"N, 87º27'24"E	Monzonitic granite		293.1 ± 1.8			

* data from Yin et al.(2017)

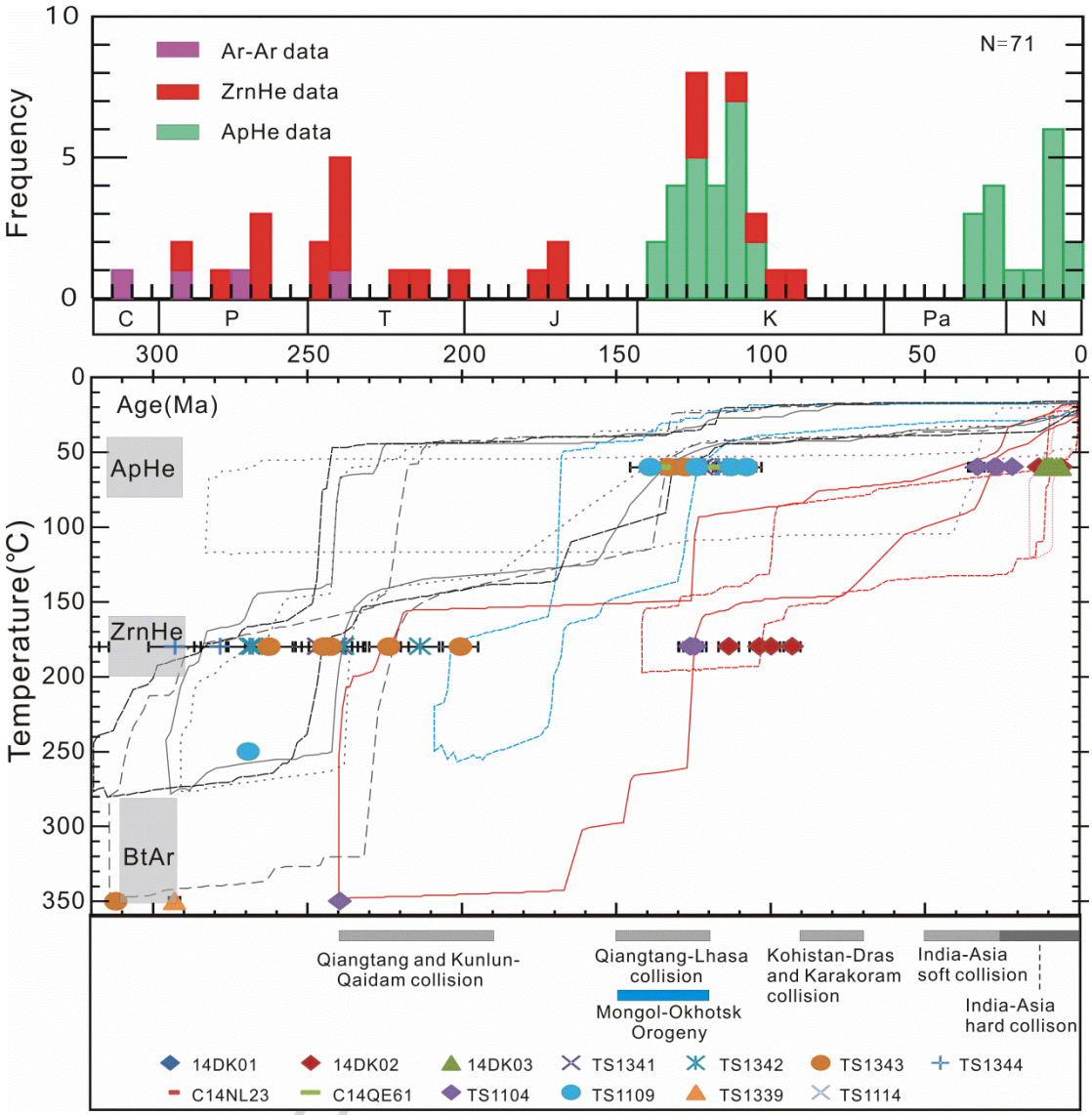

Graphical abstract

Highlights

- This paper presents new U/Pb, $^{40}Ar/^{39}Ar$, and (U-Th)/He ages on samples from Chinese Tianshan granitoids.
- Five main exhumation episodes were distinguished in the study area.
- Multi-method chronometry records a complex, punctuated accelerated cooling.
- These exhumations were related to Mesozoic Cimmerian blocks and Cenozoic India-Eurasia collisions.